Hindawi Publishing Corporation
Journal of Nanotechnology
Volume 2012, Article ID 483976, 7 pages
doi:10.1155/2012/483976

Research Article

Permeability of Electrospun Superhydrophobic Nanofiber Mats

Sarfaraz U. Patel, Gabriel M. Manzo, Shagufta U. Patel, Prashant S. Kulkarni, and George G. Chase

Department of Chemical and Biomolecular Engineering, University of Akron, Akron, OH 44325-3906, USA

Correspondence should be addressed to George G. Chase, gchase@uakron.edu

Received 14 September 2011; Accepted 14 January 2012

Academic Editor: Andrei Kolmakov

This paper discusses the fabrication and characterization of electrospun nanofiber mats made up of poly(4-methyl-1-pentene) polymer. The polymer was electrospun in different weight concentrations. The mats were characterized by their basis weight, fiber diameter distribution, contact angles, contact angle hysteresis, and air permeability. All of the electrospun nonwoven fiber mats had water contact angles greater than 150 degrees making them superhydrophobic. The permeabilities of the mats were empirically fitted to the mat basis weight by a linear relation. The experimentally measured air permeabilities were significantly larger than the permeabilities predicted by the Kuwabara model for fibrous media.

1. Introduction

Superhydrophobic properties of electrospun nanofiber mats are of interest for a number of applications. In fabrics and filters, the air permeability, in addition to their hydrophobicity, is important. Few publications report on the permeability of such mats. In this paper, we report on the measured air permeability and compare it with the permeability predicted using a common correlation for fibrous media.

Superhydrophobic surfaces are indiscriminately defined as surfaces with water contact angles (WCAs) greater than 150 degrees. Many examples of superhydrophobic surfaces are observed in nature. A well-known example of superhydrophobic surface is lotus leaf. Barthlott and Neinhuis [1] studied the lotus leaf and found that the rough-surface microstructures on the lotus leaf help the leaf to repel water off the surface, keeping it clean. In another example, Gao and Jiang [2] showed that a pond skater is able to walk on the water because of the surface structure of the legs. The legs have microhairs and nanoscaled grooves on the leg hairs, making the leg surfaces superhydrophobic. Conventionally, superhydrophobic surfaces are fabricated by creating a nanoscaled roughness on the surface and by making the surface out of low surface energy materials. Plasma etching [3], mechanical stretching [4], and electrospinning are some of the methods employed to create rough surfaces. Low surface energy compounds, typically fluorinated [5] or silicone compounds [6], have been used to create superhydrophobic surfaces. Superhydrophobic surfaces are characterized by WCA but in some applications contact angle hysteresis and critical tilt angle between the substrate and the horizontal, below which the water droplet begins to move upon elevating one end of the substrate, are also necessary [7]. It is desired to have a large contact angle and small tilt angle for self-cleaning applications.

Electrospinning is a simple and convenient method to create rough surfaces at the appropriate scale for superhydrophobicity. The method of electrospinning nanofiber mats is well documented [8]. Electrospun nanofibers are versatile materials with use in many industries including air and liquid filtration [9], tissue engineering [10], catalysis [11], and sensors [12].

In this work poly(4-methyl-1-pentene) was electrospun at various weight concentrations. The nanofibers were characterized for fiber morphology and fiber diameter distribution. The surfaces were tested for water contact angle, contact angle hysteresis, and air permeability. The permeability was fitted through a linear relation to the basis weight of the fiber mat. The measured permeability was compared to

Table 1: Electrospinning conditions of PFMOP.

Polymer PFMOP to solvent concentration % wt/wt	Solvents	kV	Tip to collector Distance (cm)	Flow rate (mL/h)	Fiber diameter range (nm)	Log normal mean diameter (nm)	Log normal standard deviation
1%	Cyclohexane-Acetone-DMF (80/10/10 by weight)	20	15	15	50–700	193	0.488
2%		20	15	15	150–680	350	0.276
3%		20	15	15	150–1500	618	0.500
4%		20	15	15	210–1400	707	0.407

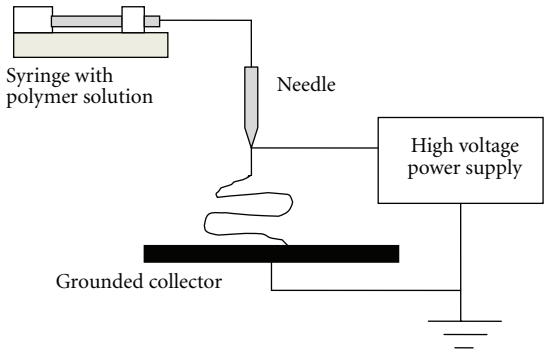

Figure 1: Schematic of a laboratory electrospinning setup.

permeability calculated from a published correlation for fibrous media.

2. Experimental Description

2.1. Materials. Poly(4-methyl-1-pentene) (PFMOP) with melt index 26 g/10 min at 230°C at a load of 2.16 kg (ASTM D 1238) was purchased from Aldrich. The PFMOP may be dissolved in a number of solvents. Through some trial, and error the combination of three solvents (cyclohexane, acetone, and N-N-dimethylformamide (DMF)) mixed in a ratio of 80/10/10 by weight gave consistent electrospun nanofiber mats. The solvents were purchased from Fisher Scientific and were used without any further purification. PFMOP was dissolved in the solvent mixture at 70°C to prepare electrospinning solutions with polymer concentrations ranging from 1% to 4% by weight. Mild stirring was used to make all electrospinning solutions. The syringes used for electrospinning were preheated at 70°C for about 20 minutes and then used for electrospinning.

2.2. Electrospinning. Figure 1 shows schematics of the electrospinning set-up employed in this work. The polymer solution was fed to a preheated 5 mL plastic syringe equipped with a 21-gauge needle via syringe pump (SP220i World Precision Instruments, USA) at feed rate of 15 mL/hr. A high voltage power supply (Gamma High Voltage Research, Ormond Beach, Fl, USA) was used to generate potential difference of 20 kV between needle and a glass slide placed on grounded aluminum foil placed at a distance of 15 cm from needle tip.

2.3. Characterization. The morphologies of the electrospun nanofibers mats were evaluated using filed emission scanning electron microscopy (JSM-7401F JEOL Ltd). The samples were silver coated for 25 seconds to minimize charging effect. The fiber diameters were observed from electronic FESEM images using ImageJ analysis software. The software and description of the software is available at the web site in [13]. Water contact angle and contact angle hysteresis were measured using the DSA20E (Krüss GmbH, Germany) at room temperature. Water drops of 5 microliter volumes were used for water contact angle measurements in air.

The permeabilities of the nanofiber mats were measured using the Frazier Air Permeability Tester (Frazier Precision Instrument Company, Inc., Md, USA). The permeability tests were conducted on electrospun nanofiber mats supported by a metal wire mesh. The wire mesh was made up of 0.09 inch diameter stainless steel wires with 25 wires per centimeter. The permeability of the wire mesh alone, with no nanofibers, was not measureable (very high permeability); hence the measured permeability of the nanofiber mat and wire mesh composite was attributed to the nanofiber mat alone.

3. Results and Discussion

The morphology of electrospun nanofibers and their spinnability are strongly affected by the electrospinning parameters including the solution properties and the surrounding environment [14]. Usually three typical morphologies such as beads, bead-on-string structure, and fiber structure can be obtained by adjusting the solvent type, solvent-to-polymer concentration, solvent additives (use of non solvents to improve volatility and polarity of solution), polymer molecular weight, temperature, and the applied voltage. Different polymer concentrations of the same polymer were used in this work to generate nanofiber structures with beads. Generally, beads are produced when the spinning solution has low polymer concentration, high surface tension, low viscosity, and low electrical conductivity [15]. Concentrations of 1, 2, 3, and 4 weight percent of PFMOP dissolved in a solvent mixture of cyclohexane/acetone and DMF (80/10/10 by weight) were electrospun to produce nanofibers. The details of electrospinning conditions are given in Table 1. SEM images and frequency distribution of PFMOP nanofibers are shown in Figures 2, 3, 4, 5, and 6.

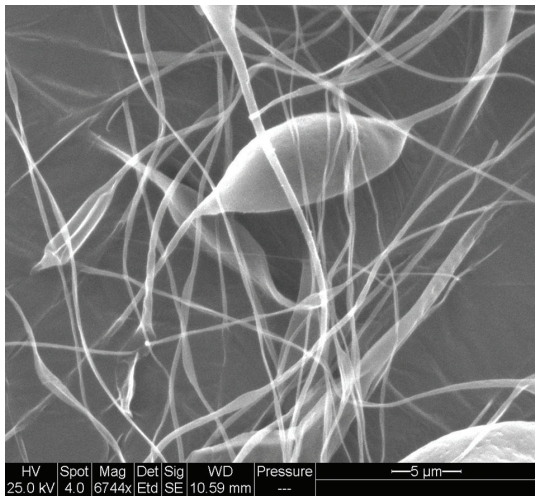

Figure 2: SEM image of 1% PFMOP nanofibers.

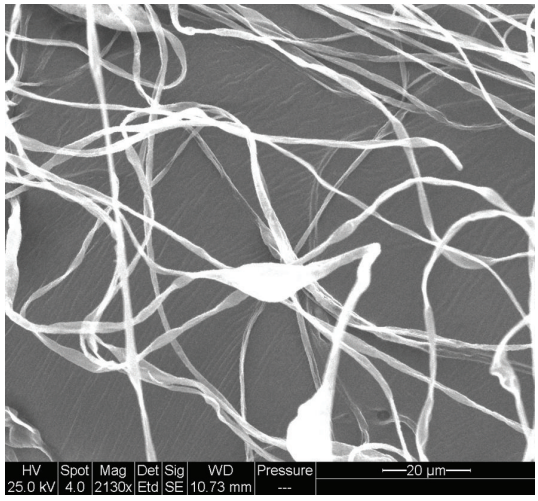

Figure 3: SEM image of 2% PFMOP nanofibers.

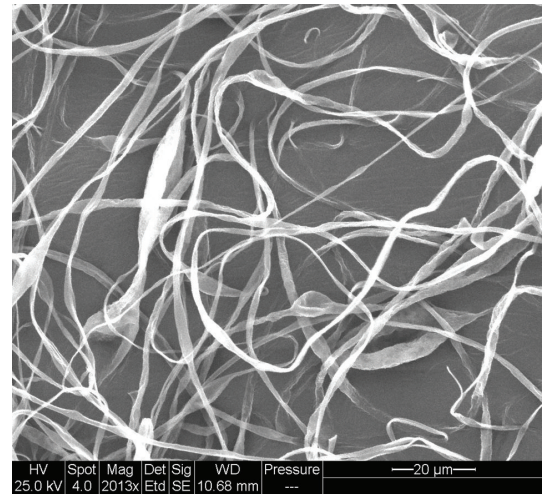

Figure 4: SEM image of 3% PFMOP nanofibers.

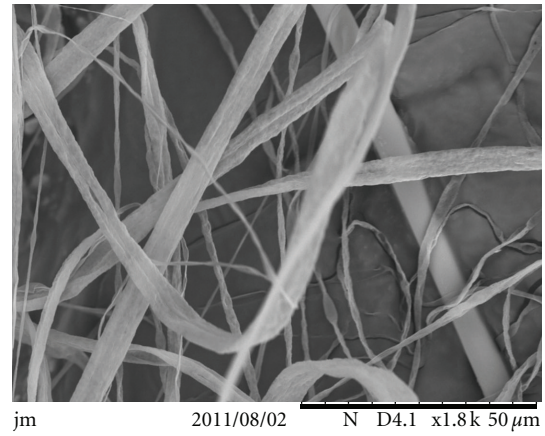

Figure 5: SEM image of 4% PFMOP nanofibers.

Figures 2–5 show that the fibers had beads. The number of beads per unit area was fairly low, so the beads were ignored in the fiber diameter distribution calculations. The images also show that some of the larger fibers were flat and ribbon shaped. The projected thicknesses of the ribbons were used as the fiber diameters though other methodologies may exist for characterizing the fiber size and shape. The projected fiber size is most relevant to superhydrophobic properties of the mat due to the Cassie-Baxter mechanism [16]. The fiber diameter distribution was calculated using a length-weighted basis and assumed a log-normal distribution curve [17]. The mean and standard deviations of the fiber sizes are listed in Table 1.

The Cassie-Baxter mechanism occurs when a droplet sits on a rough surface in contact with solid and gas at the same time. In the case of the nanofiber mats, the drops are in contact with the solid polymer fibers and air in the pore spaces between the fibers. The net effect that is the drop does not experience the same forces it normally would if

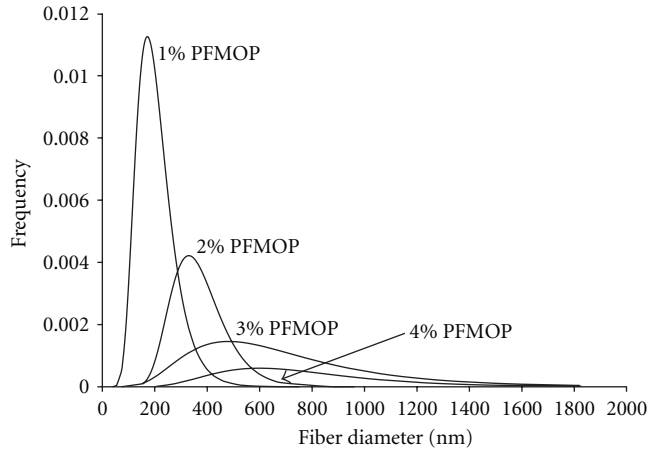

Figure 6: Nanofiber diameter frequency distribution.

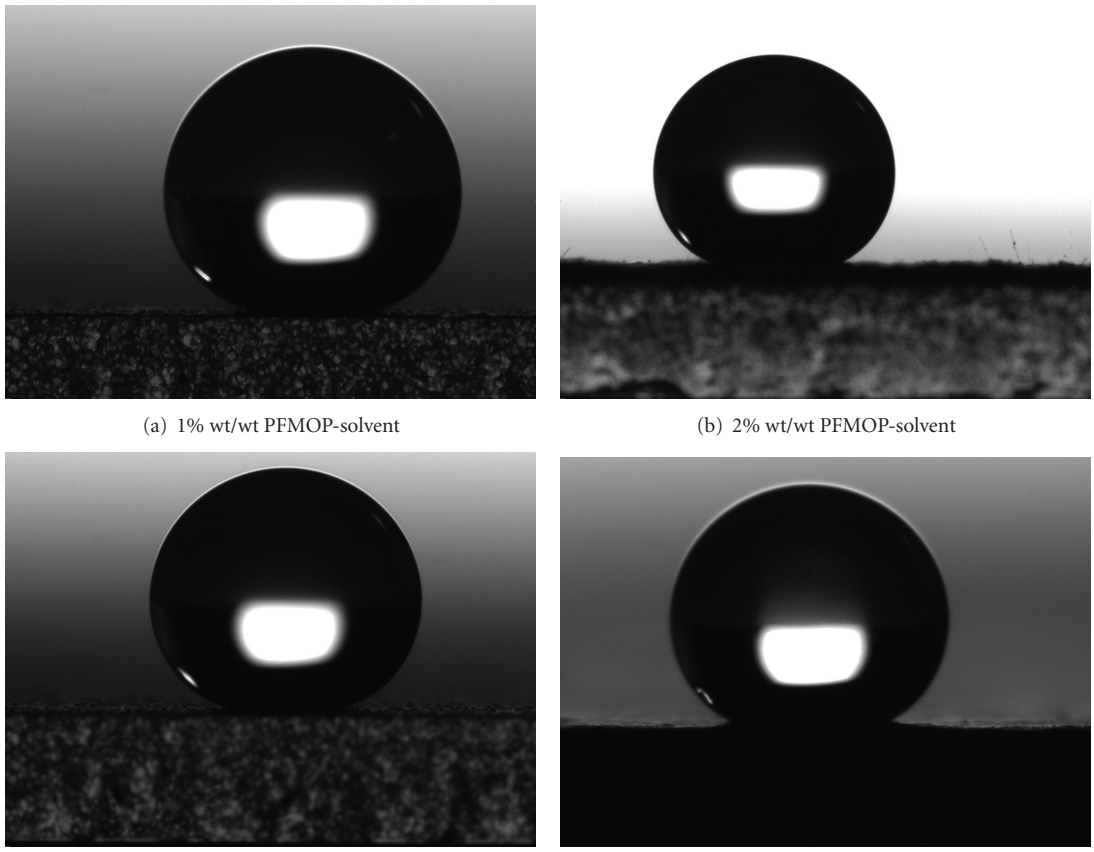

(a) 1% wt/wt PFMOP-solvent

(b) 2% wt/wt PFMOP-solvent

(c) 3% wt/wt PFMOP-solvent

(d) 4% wt/wt PFMOP-solvent

Figure 7: Photos of water drops on electrospun fiber mat surfaces from different polymer-solvent solution concentrations.

the surface was a solid smooth continuous surface instead of the porous fiber membrane and the droplet can have a contact angle exceeding 150 degrees showing superhydrophobic properties. The superhydrophobic performance of electrospun nanofiber mats is discussed in a review article by Shirtcliff et al. [18] and by Asmatulu et al. [19].

The water contact angles were measured on the DSA20E using deionized water to position 5 microliter water drops on the fiber mat surfaces. The 5 microliter drops had diameters of about 2.1 mm. At least 5 independent observations were averaged to determine the final contact angle and contact angle hysteresis value of the electrospun nanofibrous surfaces. Example images of the drops on the surfaces are shown in Figure 7.

Contact angle hysteresis is defined as the difference between the advancing and receding contact angles. A water drop of about 3 microliters was placed on the nanofiber mat and was steadily injected by the syringe until the drop volume of 5 microliters was obtained. The advancing contact angle was observed as the water was injected and the drop diameter increased. Similarly, water was steadily extracted from a 5-microliter water drop to observe the receding contact angle. The measured WCA and hysteresis for the fiber mats are listed in Table 2. The values of hysteresis as well as contact angle do not change significantly with the increase in basis weight (mass of fibers per area of mat). Relatively low values (less than 10 degrees) of hysteresis indicate that electrospun surfaces are fairly homogenous in nature and there is little interaction between water and the surface.

Table 2: WCA and hysteresis results.

Polymer PFMOP to solvent concentration % wt/wt	Basis Weight (g/m^2)	WCA (degrees)	Hysteresis* (degrees)
1%	10	162 ± 1.87	3
1%	20	160.6 ± 1.35	4
1%	30	161.7 ± 2.62	4
2%	10	161 ± 2.33	4
2%	20	161.1 ± 1.35	6
2%	30	159.8 ± 2.56	6
3%	10	162 ± 2.98	5
3%	20	160 ± 1.46	6
3%	30	159.2 ± 2.11	8
4%	10	155 ± 1.46	7
4%	20	153.3 ± 1.66	8
4%	30	153.1 ± 1.98	8

*Hysteresis is the number of degrees difference between advancing and receding contact angles.

Table 3: Permeability Results.

Polymer PFMOP to solvent concentration % wt/wt	Basis weight (g/m^2)	Fiber diameter (nm)	Permeability/ Thickness (k/L) (m)	Standard deviation (m)
1%	10	193	$1.00E-07$	$2.1E-09$
1%	20	193	$3.28E-08$	$1.2E-10$
1%	30	193	$2.79E-08$	$1.9E-10$
2%	10	350	$8.89E-08$	$2.0E-09$
2%	20	350	$3.98E-08$	$2.0E-10$
2%	30	350	$2.44E-08$	$3.9E-10$
3%	10	618	$7.43E-08$	$3.5E-09$
3%	20	618	$6.67E-08$	$7.7E-11$
3%	30	618	$2.53E-08$	$3.5E-10$
4%	10	707	$8.96E-08$	$1.4E-09$
4%	20	707	$5.13E-08$	$2.1E-10$
4%	30	707	$3.65E-08$	$1.6E-10$

Permeability is a measure of how easily a fluid passes through the filter medium. Air permeability of a nonwoven filter media is the measured air flow through an area of filter media at a specified pressure drop. Permeability is defined by Darcy's law [20]:

$$Q = \frac{Ak}{\mu}\frac{\Delta P}{L}, \tag{1}$$

where Q is the air flow rate, A is the filter area, k is the permeability, μ is the air viscosity, ΔP is the pressure drop, and L is the thickness of the filter medium. Because L is difficult to measure accurately for thin nonwoven filter media and all of the nanofiber samples had the same thickness within experimental error, the lumped parameter k/L is reported in Table 3. The permeability data listed in Table 3 are the average of 3 data points and the standard deviations of the three data points.

Regression analysis was performed to relate the effect of basis weight (grams of nanofibers per square meter of area) and fiber diameter to the permeability of nanofiber samples. The scatter in the data resulted in a weak correlation between permeability to the fiber diameter. However, the basis weight correlated strongly to the permeability/thickness, as shown in Figure 8. The fitted equation is

$$\frac{k}{L} = \left(-2.99 \pm 0.42 \times 10^{-9}\right)\ (\text{basis weight}) + (1.15 \pm 0.09) \times 10^{-7}. \tag{2}$$

The effects of the presence of beads and ribbon shapes of the fibers are likely causes of the lack of correlation between the permeability to the fiber diameter.

4. Comparison to Model Correlations

Correlations for predicting pressure drop for flows through nonwoven fiber media are available in literature. One of the more well-known correlations is Kuwabara model [21]. The Kuwabara model has been generalized to account for aerodynamic slip [22] which occurs for air flow through media of submicron-sized fibers. The pressure drop is related to the flow rate by the following expression:

$$\Delta P = \frac{16\mu cLQ(1 + 1.996\text{kn})}{d^2A[-(1/2)\ln(c) - 0.75 + c - c^2/4 + 1.996\text{kn}((-1/2)\ln(c) - .025 + c^2/4)]}, \tag{3}$$

where d is the fiber average diameter, c is the fiber volume fraction, and kn is the Knudsen number, given by

$$\text{kn} = \frac{2\lambda}{d}, \tag{4}$$

where λ is the molecular mean free path of the gas phase. By rearrangement and comparison with (1), an expression for the permeability/length is obtained as

$$\frac{k}{L} = \frac{d^2\left[-(1/2)\ln(c) - 0.75 + c - c^2/4 + 1.996\text{kn}\left((-1/2)\ln(c) - 0.25 + c^2/4\right)\right]}{16cL(1 + 1.996\text{kn})}. \tag{5}$$

For room temperature and 1 atm of pressure, the mean free path of air is 69 nm. The fiber volume fraction is related to the mat basis weight by

$$c = \frac{(\text{basis weight})}{L(\text{fiber density})}. \tag{6}$$

To make an estimate of the permeability/thickness based on the generalized Kuwabara model, the filter thickness is taken to be the average mat thickness of about 65 microns. The density of PFMOP is 0.84 g/cc, as reported by the polymer supplier at their web site in [23]. The data in Figure 9 are plotted along with curves from (5) as shown in Figure 9.

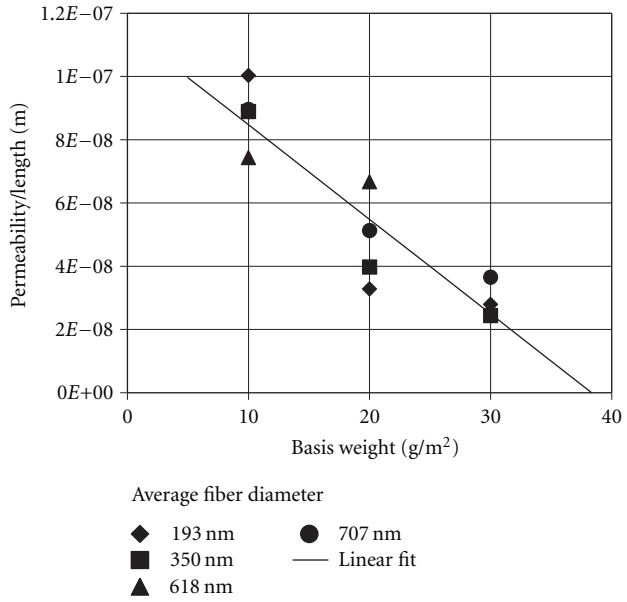

Figure 8: Linear fit of basis weight to the permeability/length. The linear fit is given in (2). The average diameters of the fibers are indicated by the data points for each basis weight.

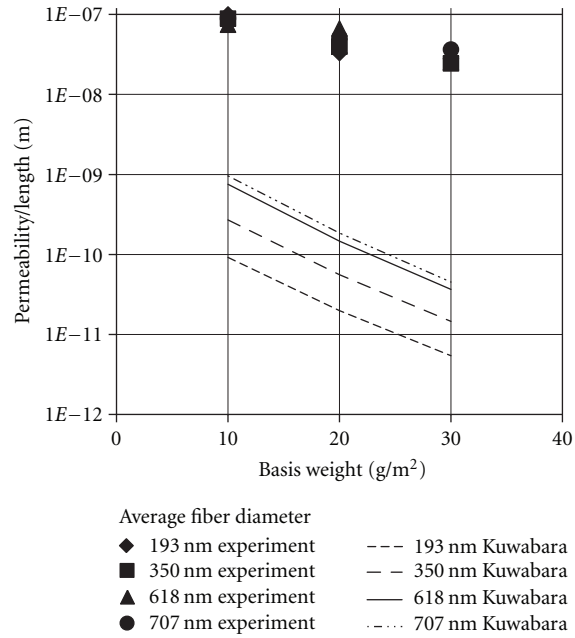

Figure 9: Experimental data plotted in comparison to the calculated values using the Kuwabara model.

Figure 9 shows that the calculated permeability/thickness is about two to three orders of magnitude smaller than the measured values. The Kuwabara model assumes that the mats have volume fractions of fibers on the order of about 10% or less. For the nanofiber mats studied in this work, the fiber volume fractions ranged from 18 to 55%. Also, the Kuwabara model assumes that the flow through the pores is due to pressure-driven flow whereas the flows through very small pores may be driven by diffusion mechanisms [24].

Furthermore, the Kuwabara model assumes that the fibers are arranged in regular arrays of parallel fibers and the fibers are all cylindrically shaped with one diameter. The morphologies of the electrospun fibers and mats are randomly arranged, have different diameters and shapes, and have beads. All of these factors contribute to the significant difference between the measured and calculated permeabilities plotted in Figure 9.

This shows that models similar to the Kuwabara model may not be appropriate for modeling thin electrospun fiber. However, those models may be adequate for conditions that more closely fit the assumptions in the model, such as when the electrospun fibers are structured in a way that the fiber volume fraction is much less than 10%. The development of models for predicting permeabilities for thin electrospun fiber mats is a topic for future research.

5. Conclusions

In this work, poly(4-methyl-1-pentene) was electrospun to produce superhydrophobic mats. The morphology of the fibers and fiber diameter was evaluated for various electrospinning solution concentrations. The fibers were circular and ribbon shaped and had beads. The average fiber diameters ranged from about 200 to 700 nm as the polymer concentration increased from 1 to 4 wt%. The fiber mats were superhydrophobic with contact angles exceeding 150 degrees. The water contact angles decreased as fiber diameter increased but were not significantly affected by the fiber mat basis weight. The permeability was fitted to a linear relation to the mat basis weight but was weakly related to the fiber diameter. Comparison of the experimentally measured mat permeability to the permeability calculated using the Kuwabara model showed that the Kuwabara model underestimated the permeability by several orders of magnitude.

Acknowledgments

This work was supported by the Coalescence Filtration Nanofibers Consortium (Ahlstrom, Cummins Filtration, Donaldson, Elmarco, Hollingsworth and Vose, Parker Hannifin, and SNS Nanofiber Technology LLC).

References

[1] W. Barthlott and C. Neinhuis, "Purity of the sacred lotus, or escape from contamination in biological surfaces," *Planta*, vol. 202, no. 1, pp. 1–8, 1997.

[2] X. Gao and L. Jiang, "Water-repellent legs of water striders," *Nature*, vol. 432, no. 7013, p. 36, 2004.

[3] M. Morra, E. Occhiello, and F. Garbassi, "Contact angle hysteresis in oxygen plasma treated poly(tetrafluoroethylene)," *Langmuir*, vol. 5, no. 3, pp. 872–876, 1989.

[4] J. Zhang, J. Li, and Y. Han, "Superhydrophobic PTFE surfaces by extension," *Macromolecular Rapid Communications*, vol. 25, no. 11, pp. 1105–1108, 2004.

[5] H. Yabu and M. Shimomura, "Single-step fabrication of transparent superhydrophobic porous polymer films," *Chemistry of Materials*, vol. 17, no. 21, pp. 5231–5234, 2005.
[6] C. R. Crick and I. P. Parkin, "Preparation and characterisation of super-hydrophobic surfaces," *Chemistry - A European Journal*, vol. 16, no. 12, pp. 3568–3588, 2010.
[7] J. W. Krumpfer and T. J. McCarthy, "Contact angle hysteresis: a different view and a trivial recipe for low hysteresis hydrophobic surfaces," *Faraday Discussions*, vol. 146, pp. 103–111, 2010.
[8] D. H. Reneker and A. L. Yarin, "Electrospinning jets and polymer nanofibers," *Polymer*, vol. 49, no. 10, pp. 2387–2425, 2008.
[9] S. A. Hosseini and H. V. Tafreshi, "3-D simulation of particle filtration in electrospun nanofibrous filters," *Powder Technology*, vol. 201, no. 2, pp. 153–160, 2010.
[10] A. Karchin, F. I. Simonovsky, B. D. Ratner, and J. E. Sanders, "Melt electrospinning of biodegradable polyurethane scaffolds," *Acta Biomaterialia*, vol. 7, no. 9, pp. 3277–3284, 2011.
[11] X. Zhou, Y. Qiu, J. Yu, J. Yin, and S. Gao, "Tungsten carbide nanofibers prepared by electrospinning with high electrocatalytic activity for oxygen reduction," *International Journal of Hydrogen Energy*, vol. 36, no. 13, pp. 7398–7404, 2011.
[12] L. Sheng, C. Dajing, and C. Yuquan, "A surface acoustic wave humidity sensor with high sensitivity based on electrospun MWCNT/Nafion nanofiber films," *Nanotechnology*, vol. 22, no. 26, Article ID 265504, 7 pages, 2011.
[13] *ImageJ*, 2011, http://rsbweb.nih.gov/ij/index.html .
[14] D. Li and Y. Xia, "Electrospinning of nanofibers: reinventing the wheel?" *Advanced Materials*, vol. 16, no. 14, pp. 1151–1170, 2004.
[15] Z. Zhenxin, *Morphology and internal structure of polymeric and carbon nanofibers*, Ph.D. thesis, The University of Akron, 2011.
[16] A. B. D. Cassie and S. Baxter, "Wettability of porous surfaces," *Transactions of the Faraday Society*, vol. 40, pp. 546–551, 1944.
[17] J. S. Varabhas, G. G. Chase, and D. H. Reneker, "Electrospun nanofibers from a porous hollow tube," *Polymer*, vol. 49, no. 19, pp. 4226–4229, 2008.
[18] N. J. Shirtcliffe, G. McHale, and M. I. Newton, "The superhydrophobicity of polymer surfaces: recent developments," *Journal of Polymer Science, Part B*, vol. 49, no. 17, pp. 1203–1217, 2011.
[19] R. Asmatulu, M. Ceylan, and N. Nuraje, "Study of superhydrophobic electrospun nanocomposite fibers for energy systems," *Langmuir*, vol. 27, no. 2, pp. 504–507, 2011.
[20] L. Svarovsk, *Solid-Liquid Separation*, Butterworths, London, UK, 1990.
[21] S. Kuwabara, "The forces experienced by randomly distributed parallel circular cylinders or spheres in a viscous flow at small reynolds numbers," *Journal of the Physical Society of Japan*, vol. 14, no. 4, pp. 527–532, 1959.
[22] R. C. Brown, *Air Filtration: An Integrated Approach to the Theory and Applications of Fibrous Filters*, Pergamon Press, Oxford, UK, 1st edition, 1993.
[23] http://www.polymerprocessing.com/polymers/PMP.html .
[24] J. J. Carberry, *Chemical and Catalytic Reaction Engineering*, McGraw-Hill , New York, NY, USA, 1976.